Electronic, magnetic and optical properties of XScO₃ (X=Mo, W) perovskites

Amall Ahmed Ramanathan and Jamil Mahmoud Khalifeh

Department of Physics, School of Science, The University of Jordan, Amman, Jordan

ABSTRACT

The density functional theory (DFT) full potential linearized augmented plane wave (FP-LAPW) method with the modified Becke–Johnson (mBJ) approximation is used to perform spin polarised calculations of the transition metal perovskites $MoScO_3$ and $WScO_3$. Both depict half metallic behaviour with semiconducting and metallic in the minority and majority spins respectively. $MoScO_3$ and $WScO_3$ have indirect R– Γ band gaps in the minority spin channels of 3.61 and 3.82 eV respectively. Moreover, they both show substantial integer magnetic moments of $3\mu_B$ with 100% spin polarization typical to half metals. In addition, we calculate the dielectric function, optical conductivity and the optical constants, namely, the refractive index, the reflectivity, the extinction and absorption coefficients.

INTRODUCTION

The recent years has seen a lot of research on perovskites for potential applications in electronics, photovoltaics, renewable energy and innumerable other industries (*Mannhart & Schlom, 2010*; *Kulkarni et al., 2012*; *Hodes, 2013*). The universal structural formula of a perovskite is ABX_3 and the cubic form is the most ideal case. X atom is usually oxygen. It could also be a halide. A/B atoms are in general alkali, alkali earth, rare earth or transition metals (*Johnsson & Lemmens, 2007*; *Babu et al., 2012*). Thus, an enormous variety of structural modifications and variants are possible which can accommodate almost all of the elements in the periodic Table. The flexibility in choice of atom types gives rise to a multitude of perovskite structures with interesting electronic, magnetic and optical properties and motivates the continued interest in this family (*Hayatullah et al., 2014*; *Sesion et al., 2010*; *Aycibin & Naciye, 2017*).

Transition metals (TM) are exceptionally valuable and allow for complex magnetic interactions depending upon the local environment and dimensionality to give intriguing magnetic, magneto-electric, multiferroic, piezoelectric properties (*Ramanathan & Khalifeh, 2017*; *Cai et al., 2019*; *Wang & Zhang, 2004*) and even induce non-magnetic materials to become magnetic (*Ramanathan, Khalifeh & Hamad, 2009*; *Ramanathan, Khalifeh & Hamad, 2011*). Thus, transition metal (TM) perovskites are of special interest and past research show a wide range of electronic, magnetic and optical properties owing to the complex nature of TM ion interactions with oxygen or halides (*Kimura et al., 2003*;

Corresponding author
Amall Ahmed Ramanathan,
a.ramanathan@ju.edu.jo

Kovalenko, Protesescu & Maryna, 2017). It is mainly the unfilled or filled 'd' bands of the TM that are responsible for the electronic/magnetic and dielectric properties respectively.

In most of the previous studies on TM perovskites, the TM occupies the B site. Recently, we explored the effect of 3d-filling on the electronic, magnetic and optical properties on $TMScO_3$ perovskites where the TM (from Ti to Zn) sits on the A site (*Mahmoud et al., 2020*). The materials show half metallic behavior with wide band gaps, except for $TiScO_3$ and $VScO_3$ which are metallic and semiconducting. As, a further study, in the current work we explore the electronic, magnetic and optical properties with TM Mo and W which are isoelectric to Cr in group VI i.e. $MoScO_3$ and $WScO_3$ perovskites. The purpose of the paper is to give the essential and accurate theoretical information of the optoelectronic properties of these perovskite compounds, which are being investigated for the first time for possible technological applications and further research.

The perovskites $MoScO_3$ and $WScO_3$ are investigated from first principles using the full-potential linearized augmented plane wave (FP-LAPW) density functional theory (DFT) method with the wien2k software program. We have used the mBJ exchange potential as DFT-mBJ is a powerful tool and predicts the important electronic and band-structure related properties with high degree of accuracy.

The paper is arranged as follows: "Materials & Methods" gives the Calculation details, "Results" is devoted to the Discussion of results under the sub headings_ Structural and electronic; Magnetic and Optical properties, finally "Conclusions" presents the Conclusions.

MATERIALS & METHODS

The full-potential linearized-augmented plane wave (FP-LAPW) method as implemented in the WIEN2k (*Blaha et al., 2020*) code based on DFT (*Kohn & Sham, 1965*) is used to calculate the spin polarized ground states of the perovskites. We have used generalized gradient approximation (GGA) of Perdew, Burke and Ernzerhof (PBE) (*Perdew, Burke & Ernzerhof, 1996*) to calculate the optimized structures at a $10 \times 10 \times 10$ kpoint grid. The optimized lattice constant values have then been used with the more accurate Modified Becke-Johnson (mBJ) exchange correlation of Trans Blaha (*Tran & Blaha, 2009*) to evaluate the electronic, magnetic and optical properties using denser grids of $15 \times 15 \times 15$ and $30 \times 30 \times 30$ for electronic/magnetic and optical properties respectively.

In order to achieve energy eigenvalues convergence, the wave functions in interstitial region were expanded in plane waves with a cutoff of Rmt^*Kmax set to 8; Kmax gives the magnitude of the largest K vector in the plane-wave expansion. The muffin-tin radius (RMT), which denotes the smallest atomic sphere radius is taken to be 2.5 and 2.7 a.u for Mo, W respectively and 1.60 a.u for Sc and O atoms. The Brillouin zone integrations within the self-consistency cycle are performed via a tetrahedron method (*Blöchl, Jepsen & Andersen, 1994*) using 120 k points in the irreducible wedge of the Brillouin zone (IBZ) for all compounds. The self-consistence calculations have convergence tolerance thresholds of less than 10^{-4} Ry in energy and 10^{-4} in electron charges.
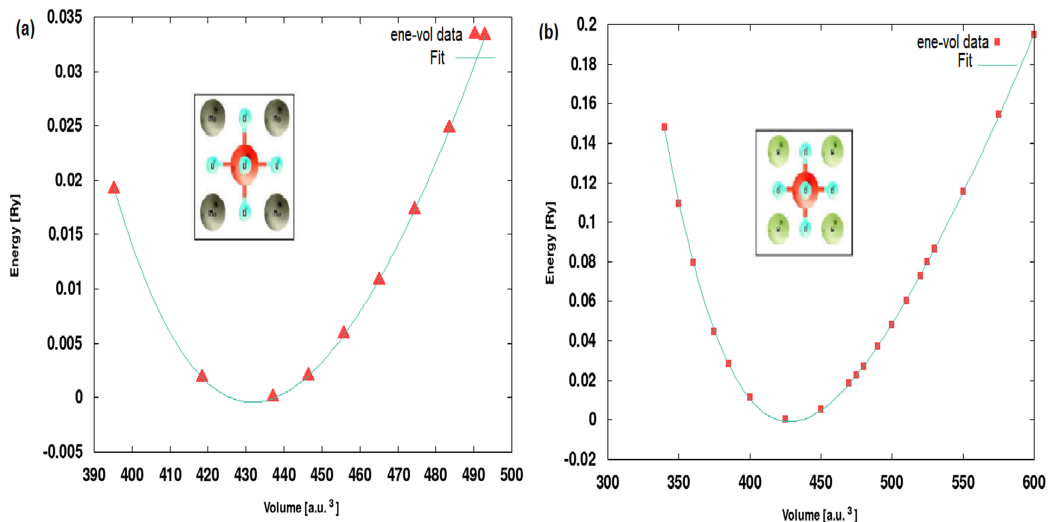
Figure 1 Optimised structures. The energy-volume optimization showing the Murnaghan fit curves for (A) MoScO$_3$ and (B) WScO$_3$.

RESULTS

Structural and electronic properties

The MoScO$_3$ and WScO$_3$ Perovskites in the cubic form with space group is Pm-3m (#221) contain one formula unit and the Mo/W, Sc and O atoms are positioned at 1a (0, 0, 0), 1b (½, ½, ½) and 3c (0, ½, ½) sites of Wyckoff coordinates, respectively.

The lattice constants of XScO$_3$ structures are optimized using Murnaghan equation of state (*Murnaghan, 1944*) and the energy vs volume curves are presented in Fig. 1 along with the structure visualization. The energies have been shifted by the minimum energy value which is set to zero in the plot. Since, the structure is cubic only volume optimization is required.

The optimized lattice constants and bulk moduli at the equilibrium minimum energy ground state are shown in Table 1. We notice from the Table that the lattice constant of the perovskites decreases slightly with increasing atomic numbers of the TM. Although, the individual ionic radii of Mo and W are comparable the decrease in size of the compounds can be attributed to the change in electronic density and changes in the occupation of the band orbitals in new molecular environment.

The thermodynamic stability of the perovskites is important for the existence and synthesis of these compounds. We have evaluated the energies of formation E$_{form}$ for the perovskites to give an indication of their stability and these values are presented in Table 1. The energy of formation is obtained by using Eq. (1) below:

$$E_{form} = E_{XScO_3}^{Bulk} - E_X^{Bulk} - E_{Sc}^{Bulk} - 3E_O^{free} \tag{1}$$

where, E_{form} is the formation energy of the perovskite; X = Mo/W; $E_{XScO_3}^{Bulk}$; E_X^{Bulk} and E_{Sc}^{Bulk} are the bulk equilibrium total energies of the XScO$_3$ compound, the TM element and Sc respectively; and E_O^{free} is the free energy of a single oxygen atom. The E$_{form}$ obtained for

Table 1 The optimized Structural parameters for the XScO₃ perovskites.

Perovskites	Lattice constant a [Å]	Bo [GPa]	E_{form} [Ry]	Elastic constants (GPa)		
				C_{11}	C_{12}	C_{44}
MoScO₃	4.000	153.197	−1.958	282.2	83.5	19.8
WScO₃	3.988	157.798	−1.848	242.3	122.3	15.9

MoScO₃ and WScO₃ are −1.958 and −1.848 Ry respectively. The negative values of formation energy indicate that the perovskites are energetically stable and can be easily synthesized experimentally.

In addition to the thermodynamic stability, the mechanical/structural stability of the perovskites is an essential factor that needs to be evaluated. The dynamic stability of a crystal is measured by its response to deformations and the evaluation of the elastic energy viz the elastic constants. If a system is deformed under equilibrium conditions arbitrarily through a small strain "e", the change in energy would be as denoted in Eq. (2) below (*Mouhat & Coudert, 2014*).

$$U_{elast} = \frac{V}{2} \sum_{ij=1}^{6} C_{ij}e_ie_j + \text{higher order terms(HO)} \qquad (2)$$

The number of independent elastic constants in a crystal is dictated by symmetry of the system. For cubic symmetry as in the present study only three independent elastic constants C_{11}, C_{12} and C_{44} are required to confirm the stability and the above equation is reduced to

$$U_{elast} = \frac{V}{2}(C_{11} - C_{12})(e_1^2 + e_1^2 + e_1^2) + C_{12}(e_1 + e_2 + e_3)^2 + C_{44}(e_1^2 + e_1^2 + e_1^2) + HO \qquad (3)$$

The system will be dynamically stable if U_{elast} is positive i.e. the deformed system is at a higher energy. This condition restricts the values of elastic constants, which are the necessary stability conditions of Born (*Born, 1940*); $C_{12} < B < C_{11}$; $(C_{11} - C_{12}) > 0$; $(C_{11} + 2C_{12}) > 0$ and $C_{44} > 0$.

We have obtained the second order elastic constant values by performing rigorous strain-energy calculations using the package ElaStic 1.0 (*Golesorkhtabar et al., 2013*) with the wien2k DFT code. The results for a second order fit are given in Table 1. A look at these values show that the comprehensive Born criteria holds true for both the perovskites and the mechanical dynamical stability of these perovskites is confirmed. Due to lack of previous experimental or theoretical works on these new perovskites we cannot compare our results for the thermodynamic or mechanical stability.

The dynamic stability of a crystal also requires that all the phonon frequencies in the spectra are positive and that there are no imaginary or soft phonon modes. We have investigated the phonons at the gamma point (zone center) by performing a density functional perturbation theory (DFPT) calculation using the Quantum Espresso code (*Baroni et al., 2001*) with projector augmented wave (PAW) pseudopotentials and the
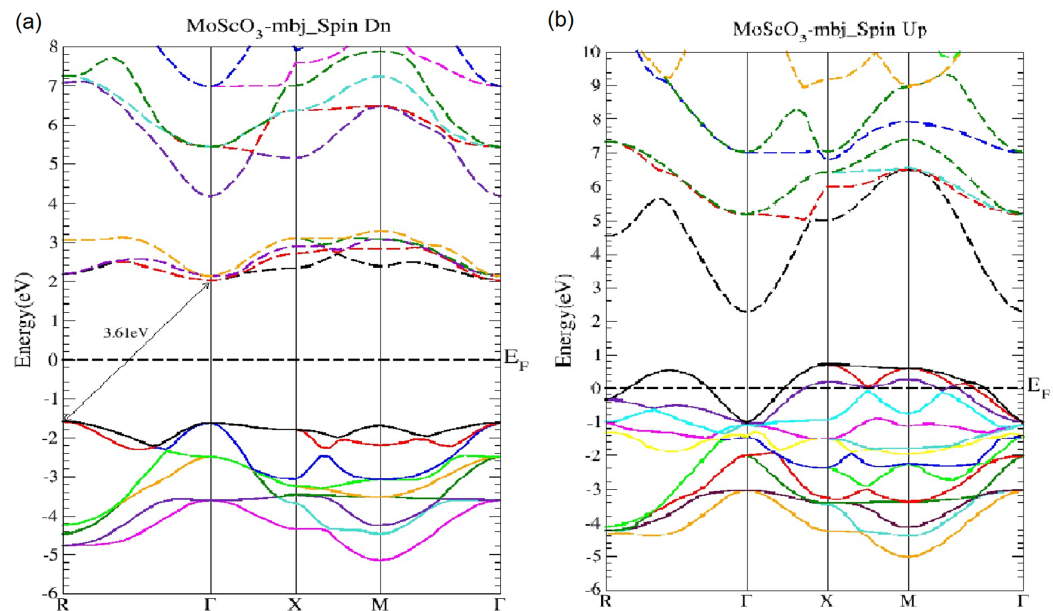
Figure 2 MoScO₃ mBJ band structure. The $MoScO_3$ electronic band structures for (A) the minority (Spin Dn) and (B) the majority (Spin Up) channels.

GGA-PBE exchange correlation (*Perdew, Burke & Ernzerhof, 1996*). Fully relaxed structures and very stringent convergence thresholds of 10^{-22}Ry are used for highly precise and accurate results. The results for both the perovskites show the presence of imaginary phonon frequencies (negative values) at Γ point and indicate dynamic instability as seen from Table S1 of supplementary information. This implies the possibility of lower order symmetry phases and could indicate the presence of interesting ferroelectric order. More detailed experimental and theoretical investigations with full phonon dispersions for cubic as well other lower order structures are required to confirm these results and is a strong motivation for future work on these perovskites. For the sake of comparison by experimentalists we have included the simulated powder diffraction patterns of these perovskites in the supplementary information Fig. S1.

The electronic and optical calculations have been performed using the mBJ exchange functional to obtain highly accurate band structures of the perovskites and very reliable results for all the optical properties under investigation. The $MoScO_3$ and $WScO_3$ band structures along the high symmetry points are shown in Figs. 2 and 3 respectively.

As seen from Fig. 2, $MoScO_3$ shows interesting semi-conducting behavior in the minority spin with an indirect R–Γ bandgap of 3.61 eV which predominates over the direct Γ–Γ gap of 3.64 eV. In fact we see that the difference between valence band maximum (VBM) at the R and Γ points are very close, with just a difference of 0.033 eV.

In Fig. 3 the $WScO_3$ band structures are depicted and in contrast to $MoScO_3$ we see a more pronounced half metallic behavior. The minority band shows an indirect R–Γ gap of 3.82 eV and the majority spin band is strongly metallic with valence bands deep in the conduction band. Table 2 presents a summary of the band structure results.
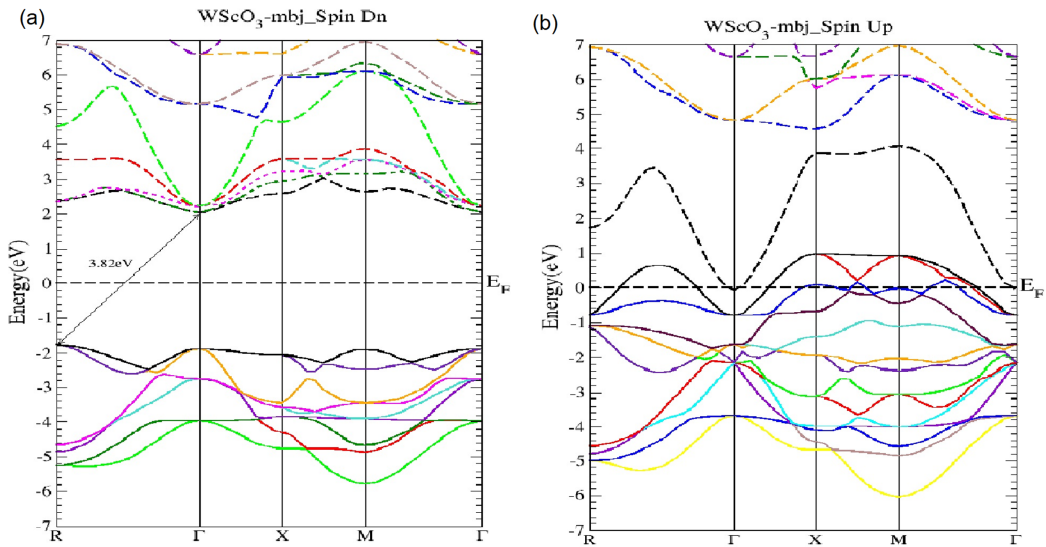
Figure 3 The WScO₃ mBJ band structure. The $WScO_3$ electronic band structures for (A) the minority (Spin Dn) and (B) the majority (Spin Up) channels.

Table 2 The mBJ electronic band gaps in the minority and majority spin channels for the $XScO_3$ perovskites.

Pervoskite $XScO_3$	Band-gap [eV]			
	Minority		**Majority**	
$MoScO_3$	R– Γ	3.61	Slightly	No gap
	Γ– Γ	3.64	Metallic	
$WScO_3$	R–Γ	3.82	Metallic	No gap
$CrScO_3$	Γ– Γ	5.496	Metallic	No gap

Magnetic properties

Although the TM are paramagnetic and individually do not show any magnetism, the Mo/WScO₃ perovskites are magnetic. The spin polarized total density of states (TDOS) plots is shown in Figs. 4 and 5 for MoScO₃ and WScO₃ respectively.

The TDOS of the minority spin of the compound shows clearly the energy gap, with the Mo DOS dominating the conduction band and oxygen states on the valence side of the TDOS. Meanwhile for the majority spin the TDOS of the compound and Mo and O DOS have peaks around E-Fermi, clearly indicating a metallic behavior for MoScO₃ majority spin state.

The TDOS for WScO3 in Fig. 5 shows a similar trend as in MoScO₃, with minority spin showing the band gap and semiconducting nature, while, the majority TDOS has prominent peaks at E-Fermi belonging to the full compound, Mo and O indicating the metallic behavior and showing consistency with the band structure plots Figs. 2 and 3. In addition, we notice, that the TDOS for both the perovskite compounds in Figs. 4 and 5 shows a marked difference in the spin up and spin down density and this clearly gives rise to the magnetism with a magnetic moment of 2.99μ₈ in the two perovskites as shown
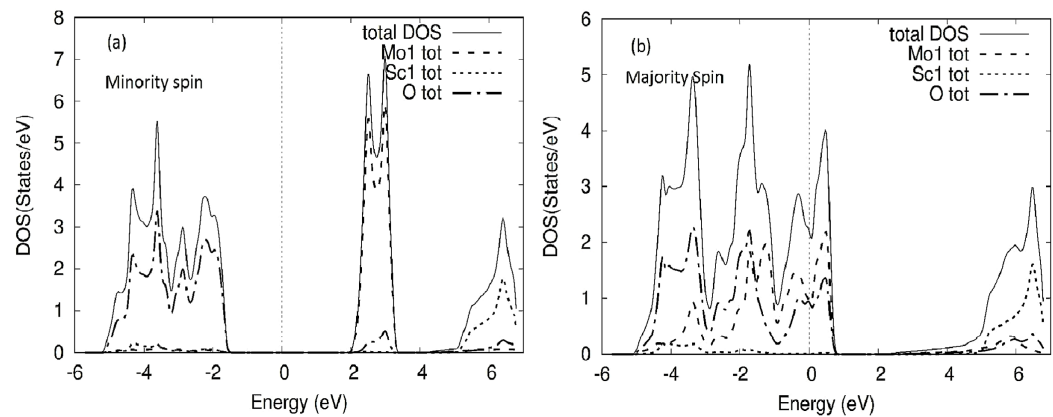
Figure 4 MoScO₃ TDOS. The MoScO₃ electronic total density of states TDOS for the compound and the atom constituents in (A) minority and (B) majority spin channels.
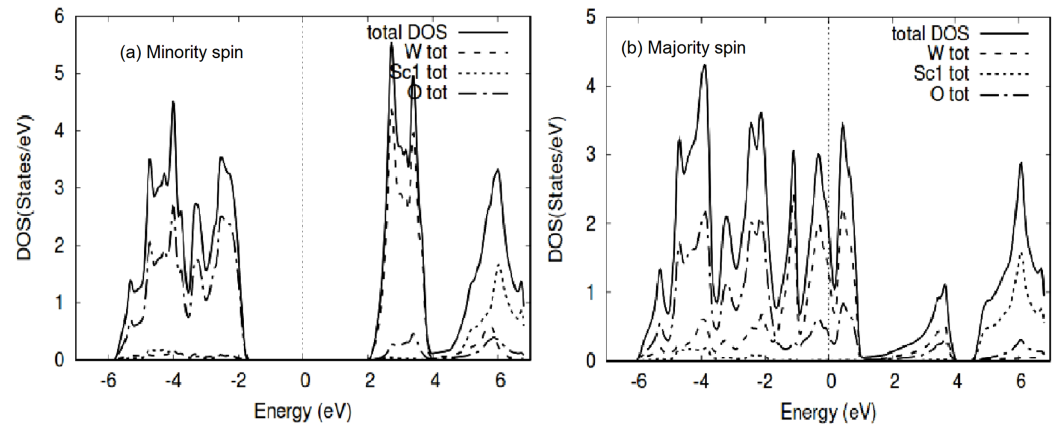
Figure 5 WScO₃ TDOS. The WScO₃ electronic total density of states TDOS for the compound and the atom constituents in (A) minority and (B) majority spin channels.

Table 3 The total magnetic moments (TDOS) of the XScO₃ perovskites: the individual atom projected, the interstitial and the complete cell values in units of μ_B.

Compound	X (Mo, W, Cr)	Sc	O	Intertitial	Total moment
MoScO₃	2.957	0.006	−0.114	0.375	2.997
WScO₃	2.996	0.012	−0.144	0.417	2.994
CrScO₃	3.536	0.004	−0.215	0.101	2.999

in Table 3 which lists the total, atom wise and interstitial magnetic moments of the perovskite compounds.

Optical properties

It is highly important to have a very dense grid and an accurate exchange correlation in the FP-LAPW to calculate the complex dielectric function that takes into account the
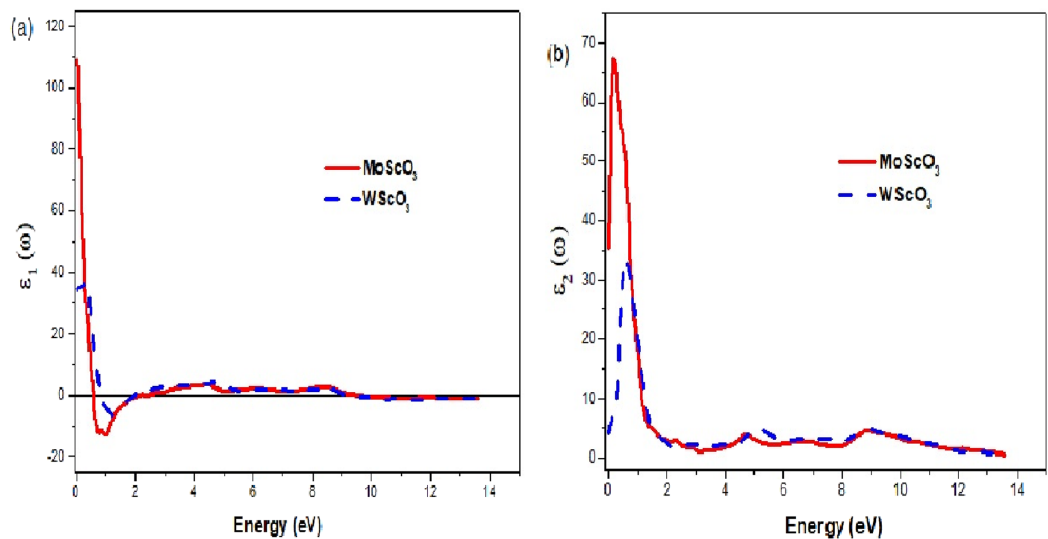
Figure 6 The Mo/WScO₃ dielectric functions. The Mo/WScO₃ dielectric functions (A) the real part $\varepsilon_1(\omega)$ and (B) the imaginary part $\varepsilon_2(\omega)$.

self-energy and local field corrections. The TB-mBJ proves to be an excellent choice with a $30 \times 30 \times 30$ grid for our optical properties calculations to obtain a high degree of accuracy of results. In this section we present the results for the dielectric function, optical conductivity and the important optical constants namely, the refractive index, the reflectivity, the extinction and absorption coefficients.

The complex dielectric function ($\varepsilon = \varepsilon_1 + i\varepsilon_2$) is a function of the amount of light absorbed by the material. The imaginary part of dielectric function, $\varepsilon_2(\omega)$, which represents absorption behavior, can be calculated from the electronic band structure of solids (*Dressel & Gruner, 2002*). The real part of dielectric function, $\varepsilon_1(\omega)$, can be calculated according to Kramers–Kroing relation (*Kramers, 1927*; *Kronig, 1926*) which represents the electronic polarization under incident light. Figure 6 shows the real and imaginary plots for the dielectric function for the Mo/WScO₃ perovskites in the photon energy range of 0–14 eV. The complex index of refraction of the medium N is defined as

$$N = \sqrt{\varepsilon} = n + ik \tag{4}$$

where, n is the usual refractive index and k is the extinction coefficient. Using the values of ε_1 and ε_2 we can obtain the refractive index n, reflectivity, and the extinction and absorption coefficients from the Eqs. (5), (6), (7) and (8).

$$R(\omega) = \frac{n + ik - 1}{n + ik + 1} \tag{5}$$

$$n(\omega) = \left[\frac{\sqrt{\varepsilon_1{}^2(\omega) + \varepsilon_2{}^2(\omega)} + \varepsilon_1(\omega)}{2} \right]^{\frac{1}{2}} \tag{6}$$
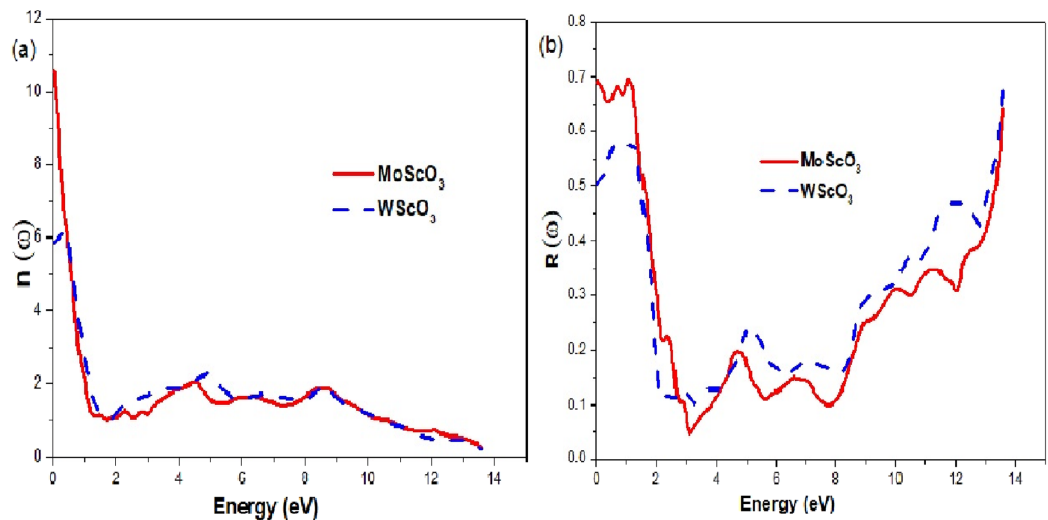
Figure 7 Mo/WScO₃ refractive index and reflectivity. The Mo/WScO₃ optical constants (A) refractive index n(ω) and (B) the reflectivity R(ω) as a function of the photon energies.

$$k(\omega) = \left[\frac{\sqrt{\varepsilon_1^2(\omega) + \varepsilon_2^2(\omega)} - \varepsilon_1(\omega)}{2}\right]^{\frac{1}{2}} \tag{7}$$

$$\alpha(\omega) = \frac{2\omega}{c}\left[\frac{\sqrt{\varepsilon_1^2(\omega) + \varepsilon_2^2(\omega)} - \varepsilon_1(\omega)}{2}\right]^{\frac{1}{2}} \tag{8}$$

The refractive index and reflectivity plots are shown in Figs. 7A and 7B respectively in the photon energy range 0–14 eV, which captures all the necessary features. Refractive index is a function of incident frequency and the graphs display maximum peak values around ω = 0, with a decrease in values as we go towards higher frequencies. Both MoScO₃ and WScO₃ have large refractive index values of 10.6 and 5.7 respectively as a result of the high electron densities in these materials (*Babu et al., 2012*). The refractive index shows an almost constant and optically isotropic behavior at high energies > orange. The reflectivity is a maximum in the visible energy range; beyond this we observe an almost constant region with very small reflectance values in 3–8 and 2–8 eV for MoScO₃ and WScO₃ respectively. This region of the spectra therefore provides good ultraviolet (UV) and higher energy absorption.

In Table 4 we list the energies of the zeros of $\varepsilon_1(\omega)$ and static values of the refractive index, the reflectivity and absorption coefficients.

The extinction coefficient and energy loss graphs are shown in Fig. 8. The extinction or attenuation coefficient relates to how strongly light of a particular wavelength is absorbed. It is an intrinsic property that depends on the chemical composition of the compound. It is a measure of the diminution of transmitted light due to scattering and absorption in the medium.

Table 4 The zero y-values of $\varepsilon_1(\omega)$ and the static optical constants at ω = zero; dielectric constant $\varepsilon_1(0)$, static refractive index n(0), static reflectivity R(0) and static absorption coefficient I(0) XScO3 perovskite compounds.

Compound	Zeros of $\varepsilon_1(\omega)$ [eV]	$\varepsilon_1(0)$	n(0)	R(0)	I(0)
MoScO$_3$	2.163 eV; 2.435	109.052	10.576	0.691	0.231
WScO$_3$	0.829; 1.946	34.329	5.869	0.504	0.351
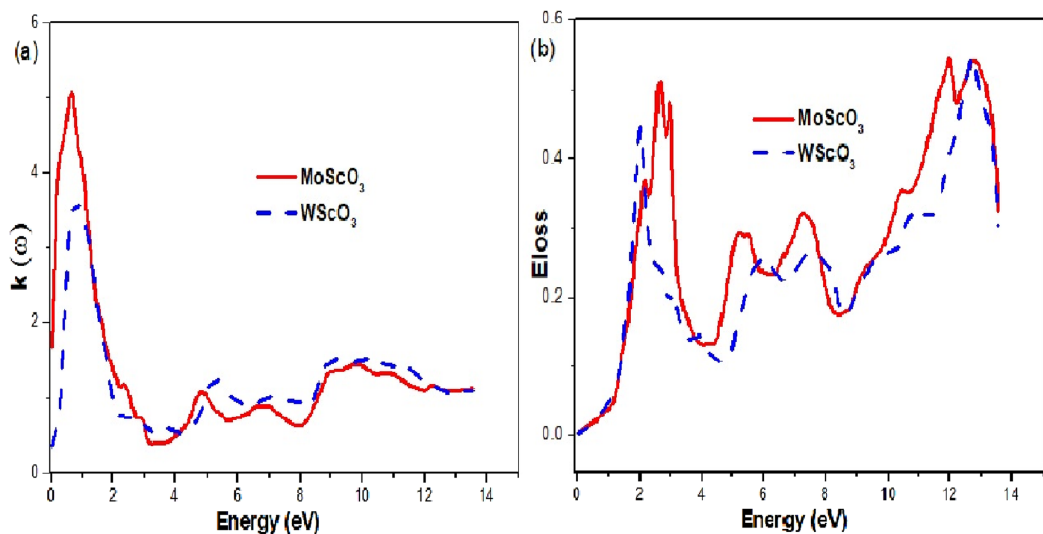
Figure 8 Mo/WScO$_3$ extinction coefficient and energy loss. The Mo/WScO$_3$ (A) extinction coefficient and (B) energy loss L(ω) as a function of the photon energies.

The electron energy loss denoted by $\alpha(\omega)$ is an important quantity and it represents the energy loss of the electron as it traverses in the medium. This function is shown in Fig. 8B. When the incident photon propagates through a polarizable dielectric or magnetic material and excites some internal degrees of freedom of the material, polaritons are formed (*Sun et al., 2016*; *Rödl & Bechstedt, 2012*). The polariton type depends on the type of elementary excitation i.e. phonon, plasmon, magnon or exiton. This is a complicated process and the peaks can be interpreted as a polariton excitation. We observe 4 peak curves for the two compounds, which occur at different characteristic energy values.

The optical conductivities and absorption coefficients are shown in Figs. 9A and 9B respectively.

The plots have 4 maximum peaks at different energy values. First, in the infra red (IR) region; the next peaks appear in the UV and above region. Similar features appear for the absorption coefficients.

DISCUSSION

The mbj exchange potential has consistently proved to give accurate and very reliable band structures comparable to that of GW or hybrid functionals. A direct bandgap is very favorable since excitation is possible with photons of energy equivalent or higher than the
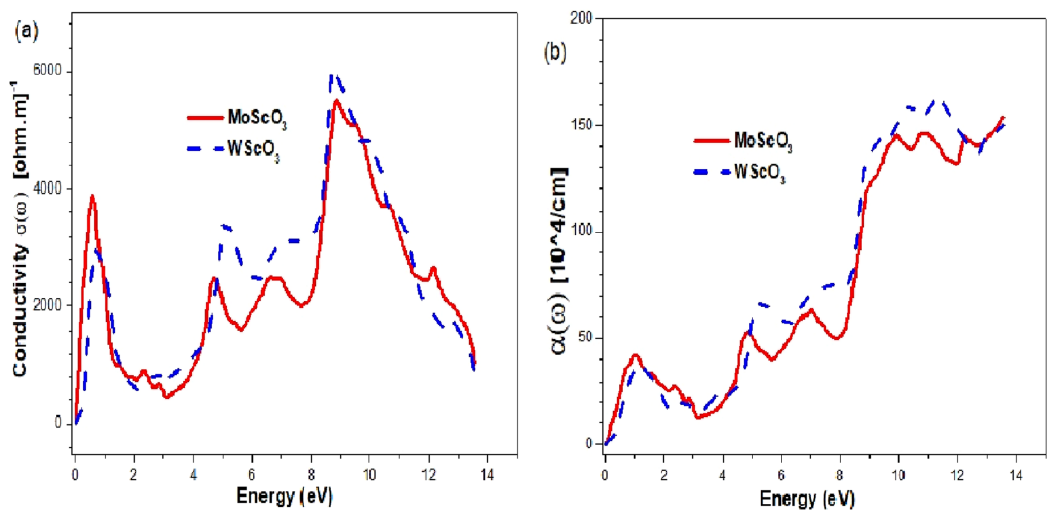
Figure 9 Mo/WScO₃ Optical conductivity and absorption coefficient. The Mo/WScO₃ (A) optical conductivity σ (ω) and (B) absorption coefficient α(ω) as a function of the photon energies.

band gap, and gives stronger emission or absorption properties for potential applications in photovoltaics (PV), light emitting diodes (LED) etc. The indirect band gap requires both a photon and phonon for excitation of electrons from the valence to conduction band; nevertheless, it has also useful applications in optoelectronics. Both the Mo and W perovskites are semiconducting in the minority channel with large bandgap values of 3.6 and 3.8 eV as seen from Table 2. The fact that the direct Γ−Γ gap is very close in energy to the indirect R−Γ gap in Mo is favorable and makes the MoScO₃ better suited for optoelectronic applications than that of W perovskite. Both the perovskites show metallic behavior in the majority channels the only difference being that the Mo perovskite shows a slight metallic behavior with only very few valence bands at the beginning of the conduction band, whereas the W shows a more pronounced metallic behavior as seen from Figs. 2B and 3B. The perovskites are therefore ferromagnetic half metals and the presence of states at the Fermi level in one spin channel and semiconducting in the other spin channel make these materials to have 100% spin polarization at the Fermi level. Such a feature has good potential for applications in spintronics (*Rostami, Afshari & Moradi, 2013*; *Mir, Seha & Gupta, 2020*).

For the sake of comparison with the isoelectric TM Cr we have included in the Table the values for CrScO₃ from reference (*Mahmoud et al., 2020*). We see in contrast to Mo and W perovskites CrScO₃ is an insulator with a very large bandgap of 5.5 eV in the minority channel and metallic in the majority spin.

The magnetic moment of the compounds arises mainly from the TM with unfilled d bands. For the sake of comparison the corresponding values for CrScO₃ has been included from reference (*Mahmoud et al., 2020*) in Table 3. The local environment and the complex interactions of the TM 'd' orbitals with the Sc and O₂ atoms gives rise to the total, atom wise and interstitial magnetic moments as observed. Sc does not seem to play any major role in the magnetism as indicated by the spin polarized total density of states

(TDOS) plots Figs. 3 and 4. We also note from the table that the perovskites have very similar total moments of ~3μ$_B$. This is as expected since Mo, W and Cr belong to the same group VI elements and are isoelectric.

Knowledge of the optical properties of a compound is crucial and fundamental for many applications and applied research. We see from the plots of the real and imaginary parts of dielectric function that the active spectral region is within 2 eV, beyond which the graphs are flat. The static dielectric constants are those at ω = 0, and we notice that the ε$_1$ value of MoScO$_3$ is more than double that of WScO$_3$ indicating a very much higher dielectric constant. The negative values for ε$_1$(ω) indicate a metal like behavior in these very low photon energies with complete reflection of light. Moreover, in Fig. 6B the ε$_2$(ω) peaks are also more than twice that of WScO$_3$, implying much higher absorption capabilities. The peaks occur at low photon energy around 1 eV and indicate transitions of valence oxygen '2p' electrons to low lying conduction 4/5d bands. These observations confirm MoScO$_3$ to have better performance than WScO$_3$ for optoelectronics.

Both MoScO$_3$ and WScO$_3$ have large refractive index values of 10.6 and 5.7 respectively as seen from Fig. 7A as a result of the high electron densities in these materials (*Babu et al., 2012*). The refractive index shows an almost constant and optically isotropic behavior at high energies > orange. The reflectivity Fig. 7B is a maximum in the visible energy range, and the materials could be used as reflective coatings in this range. Beyond this we observe an almost constant region with very small reflectance values in 3–8 and 2–8 eV for MoScO$_3$ and WScO$_3$ respectively. This region of the spectra therefore provides good ultraviolet (UV) and higher energy absorption. It is well known that the materials with band gaps larger than 3.1 eV as in the present case, work well for device applications in the UV region of the spectrum (*Maqbool, Amin & Ahmad, 2009*). After 8 eV we see steady increases to reach ~0.6 for both compounds.

Since, ε$_1$(ω) gives us information about the electronic polarizability of a material, the zero values represent the threshold values. For negative values of ε$_1$(ω), the electrons are able to completely screen the external field, which results in reflection. But, for positive ε$_1$(ω) values (frequencies higher than Plasmon frequency), the electrons do not succeed in screening the fields, which can penetrate the dielectric medium. We see from the plot shape in Fig. 8A high values of attenuation in the 0–3 eV energy range indicating maximum absorption in this region. Figure 6B also proves this point.

From the graphs in Fig. 9 we notice that both the perovskites have good optical conductivities in the visible range and also high absorption coefficients making them excellent for optoelectronic applications. They have 4 maximum peaks at different energy values. First peak, in the infra red (IR) region allows for possible use as IR detectors and sensors. The next peaks appear in the UV and above region making them appropriate for UV device applications.

CONCLUSIONS

In conclusion, this is the first investigation of the perovskites Mo/WScO$_3$ using DFT, full potential linearized augmented plane wave method with mBJ approximation to obtain accurate electronic, band structures, magnetic and optical properties. The results indicate

that the compounds are half metals with semiconducting in the minority and metallic behaviour in the majority spin channels. Moreover, the considerable band gap and sizeable magnetic moment makes these materials very suitable for spintronic applications.

In addition, the optical spectral properties in the energy range of 0–14 eV for the dielectric function and optical constants gives a very reliable and through understanding for potential applications of these materials in optoelectronics.

ACKNOWLEDGEMENTS

This work has been carried out at the theoretical physics laboratory, department of Physics at the University of Jordan. We are grateful to the deanship of academic research, The University of Jordan for the computational facility and time.

Funding
The authors received no funding for this work.

Competing Interests
The authors declare that they have no competing interests.

Author Contributions

- Amall Ahmed Ramanathan performed the experiments, analyzed the data, performed the computation work, prepared figures and/or tables, and approved the final draft.
- Jamil Mahmoud Khalifeh conceived and designed the experiments, authored or reviewed drafts of the paper, and approved the final draft.

Data Availability
Electronic band structures and DOS raw data are available at figshare: Ramanathan, Amall; Khalifeh, Jamil (2020): Electronic Band structures and Density of states of XScO3. figshare. Dataset. DOI 10.6084/m9.figshare.13295933.v1.

Optical and magnetic raw data are available at figshare: Ramanathan, Amall; Khalifeh, Jamil (2020): Optical and magnetic properties of XScO3. figshare. Dataset. DOI 10.6084/m9.figshare.13295957.v1.

Supplemental Information
Supplemental information for this article can be found online at http://dx.doi.org/10.7717/peerj-matsci.15#supplemental-information.

REFERENCES

Aycibin M, Naciye ECE. 2017. First-principles calculation of the electronic and optical properties of BiRhO3 compound AIMS. *Materials Science* **4(4)**:894–904.

Babu KE, Veeraiah A, Swamy DT, Veeraiah V. 2012. First-principles study of electronic structure and optical properties of cubic perovskite $CsCaF_3$. *Chinese Physics Letters* **29(11)**:117102.

Baroni S, de Gironcoli S, Corso AD, Giannozzi P. 2001. Phonons and related crystal properties from density-functional perturbation theory. *Reviews of Modern Physics* **73(2)**:515–562 DOI 10.1103/RevModPhys.73.515.

Blaha P, K.Schwarz FTran, Laskowski R, Madsen GKH, Marks LD. 2020. WIEN2k: an APW+lo program for calculating the properties of solids. *The Journal of Chemical Physics* **152(7)**:074101 DOI 10.1063/1.5143061.

Blöchl PE, Jepsen O, Andersen OK. 1994. Improved tetrahedron method for Brillouin-zone integrations. *Physical Review B* **49**:16223.

Born M. 1940. On the stability of crystal lattices. I. *Mathematical Proceedings of the Cambridge Philosophical Society* **36(2)**:160–172 DOI 10.1017/S0305004100017138.

Cai H, Guo Y, Gao H, Guo W. 2019. Tribo-piezoelectricity in Janus transition metal dichalcogenide bilayers: a first-principles study. *Nano Energy* **56**:33–39 DOI 10.1016/j.nanoen.2018.11.027.

Dressel M, Gruner G. 2002. *Electrodynamics of solids: optical properties of electrons in matter.* Cambridge: Cambridge University Press.

Golesorkhtabar R, Pavone P, Spitaler J, Puschnig P, Draxl C. 2013. ElaStic: a tool for calculating second-order elastic constants from first principles. *Computer Physics Communications* **184(8)**:1861–1873 DOI 10.1016/j.cpc.2013.03.010.

Hayatullah G, Murtaza R, Khenata S, Muhammad S, Reshak AH, Wong KM, Bin Omran S, Alahmed ZA. 2014. Structural, chemical bonding, electronic and magnetic properties of KMF3 (M = Mn, Fe, Co, Ni) compounds. *Computational Materials Science* **85**:402–408 DOI 10.1016/j.commatsci.2013.12.054.

Hodes G. 2013. Perovskite-based solar cells. *Science* **342(6156)**:317–318 DOI 10.1126/science.1245473.

Johnsson M, Lemmens P. 2007. Crystallography and chemistry of perovskites. Handbook of magnetism and advanced magnetic materials. *Available at https://arxiv.org/abs/cond-mat/0506606*.

Kimura T, Goto T, Shintani H, Ishizaka K, Arima T, Tokura Y. 2003. Magnetic control of ferroelectric polarization. *Nature* **426(6962)**:55–58 DOI 10.1038/nature02018.

Kohn W, Sham LJ. 1965. Self-consistent equations including exchange and correlation effects. *Physical Review* **140A(4A)**:A1133–A1138 DOI 10.1103/PhysRev.140.A1133.

Kovalenko MV, Protesescu L, Maryna I. 2017. Bodnarchuk properties and potential optoelectronic applications of lead halide perovskite nanocrystals. *Science* **358(6364)**:745–750 DOI 10.1126/science.aam7093.

Kramers HA. 1927. *Atti del Congresso Internazionale dei Fisici.* Vol. 2. Bologna: Zanichelli, 545.

Kronig RLD. 1926. On the theory of dispersion of X-Rays. *Journal of the Optical Society of America* **12(6)**:547 DOI 10.1364/JOSA.12.000547.

Kulkarni A, Ciacchi FT, Giddey S, Munnings C, Badwal SPS, Kimpton JA, Fini D. 2012. Mixed ionic electronic conducting perovskite anode for direct carbon fuel cells. *International Journal of Hydrogen Energy* **37(24)**:19092–19102 DOI 10.1016/j.ijhydene.2012.09.141.

Mahmoud NT, Almalaji BR, Mousa AA, Khalifeh JM. 2020. Effect of the3-d band filling on the structural, electronic, magnetic and optical properties of $TMScO_3$ perovskite. *Chinese Journal of Physics* **65(2)**:500–512 DOI 10.1016/j.cjph.2020.02.018.

Mannhart J, Schlom DG. 2010. Oxide interfaces: an opportunity for electronics. *Science* **327(5973)**:1607–1611 DOI 10.1126/science.1181862.

Maqbool M, Amin B, Ahmad I. 2009. Bandgap investigations and the effect of the In and Al concentration on the optical properties of InxAl1−xN. *Journal of the Optical Society of America A* **26**:2180.

Mir SA, Seha AQ, Gupta DC. 2020. New ferromagnetic half-metallic perovskites for spintronic applications: BaMO3 (M = Mg and Ca). *RSC Advances* **10**:36241–36252.

Mouhat F, Coudert FX. 2014. Necessary and sufficient elastic stability conditions in various crystal systems. *Physical Review B* **90(22)**:224104 DOI 10.1103/PhysRevB.90.224104.

Murnaghan FD. 1944. The compressibility of media under extreme pressures. *Proceedings of the National Academy of Sciences* **30(9)**:244–247 DOI 10.1073/pnas.30.9.244.

Perdew JP, Burke K, Ernzerhof M. 1996. Generalized gradient approximation made simple. *Physical Review Letters* **77**:3865.

Ramanathan AA, Khalifeh JM. 2017. Substrate matters: magnetic tuning of the Fe monolayer. *Journal of Magnetism and Magnetic Materials* **426**:450–453 DOI 10.1016/j.jmmm.2016.11.096.

Ramanathan AA, Khalifeh JM, Hamad BA. 2009. Structure and magnetism of the V/Ta(0 01) surface: a DFT calculation. *Journal of Magnetism and Magnetic Materials* **321(22)**:3804–3807 DOI 10.1016/j.jmmm.2009.07.070.

Ramanathan AA, Khalifeh JM, Hamad B. 2011. A DFT study of substrate effect on the magnetism of V(001) surface. *Surface Science* **605(11–12)**:1074–1076 DOI 10.1016/j.susc.2011.03.007.

Rostami M, Afshari M, Moradi M. 2013. Bulk and surface half-metallicity of CsS in CsCl structure: a density functional theory study. *Journal of Alloys and Compounds* **575(35)**:301–308 DOI 10.1016/j.jallcom.2013.05.171.

Rödl C, Bechstedt F. 2012. Optical and energy-loss spectra of the antiferromagnetic transition metal oxides MnO, FeO, CoO, and NiO including quasiparticle and excitonic effects. *Physical Review B* **86(23)**:235122 DOI 10.1103/PhysRevB.86.235122.

Sesion PD Jr, Henriques JM, Barboza CCA, Albuquerque EL, Freire VN, Caetano EWS. 2010. Structural, electronic and optical properties of ilmenite and perovskite CdSnO3 from DFT calculations. *Journal of Physics: Condensed Matter* **22(43)**:435801 DOI 10.1088/0953-8984/22/43/435801.

Sun Y, Xu H, Da B, Mao S-F. 2016. Calculations of energy-loss function for 26 materials. *Chinese Journal of Chemical Physics* **29(6)**:663–670 DOI 10.1063/1674-0068/29/cjcp1605110.

Tran F, Blaha P. 2009. Accurate band gaps of semiconductors and insulators with a semilocal exchange-correlation potential. *Physical Review Letters* **102(22)**:226401 DOI 10.1103/PhysRevLett.102.226401.

Wang JT, Zhang C. 2004. Magnetic field effect on dielectric properties of Pb(Fe0.5Nb0.5)O3 (PFN). *Ferroelectrics* **301(1)**:211–214 DOI 10.1080/00150190490455908.